Catalysis Today 175 (2011) 202–208

Contents lists available at ScienceDirect

Catalysis Today

journal homepage: www.elsevier.com/locate/cattod

# Titania nanotubes—A unique photocatalyst and adsorbent for elemental mercury removal

Haiqiang Wang[a,b], Siyao Zhou[a,b], Ling Xiao[a,b], Yuejun Wang[a,b], Yue Liu[a,b], Zhongbiao Wu[a,b,*]

[a] Department of Environmental Engineering, Zhejiang University, Hangzhou 310027, China
[b] Zhejiang Provincial Engineering Research Center of Industrial Boiler & Furnace Flue Gas Pollution Control, Hangzhou 310027, China

ARTICLE INFO

*Article history:*
Received 13 October 2010
Received in revised form 1 February 2011
Accepted 1 March 2011
Available online 2 April 2011

*Keywords:*
Titania nanotubes
Elemental mercury
Photocatalytic oxidation
Adsorption
Hydrothermal method

ABSTRACT

The titania nanotubes (TNTs) which generated by hydrothermal method has been used for the removal of elemental mercury ($Hg^0$) in the flue gases. Synergistic photocatalytic oxidation and adsorption were observed in this system, which resulted in an increasing tendency of removal efficiency. Results from the $Hg^0$ removal experiments demonstrated that TNTs was a wonderful catalyst and adsorbent for the removal of elelmental mercury and the removal efficiency was controlled by both morphology and crystal form of the TNTs. With calcination temperature of 500 °C, the TNTs showed the best removal performance for elemental mercury.

© 2011 Published by Elsevier B.V.

## 1. Introduction

Mercury is one of the most hazardous air pollutants for its neurological toxicity, volatility, persistence, and bioaccumulation, which pose a great threat to both human health and organism security [1–4]. Among human activities, coal combustion made the greatest contribution to anthropogenic source of mercury emission. In the coal fired flue gas, three forms of mercury may present: elemental mercury ($Hg^0$), oxidized mercury ($Hg^{2+}$) and particle bound-mercury ($Hg^P$) [5,6]. During coal combustion, elemental mercury is released and partly oxidized to $Hg^{2+}$ in the flue gas. The adsorptions of $Hg^0$ and $Hg^{2+}$ on solid surfaces (e.g., fly ash particles) lead the formation of the particle-bound mercury. Particle-bound mercury ($Hg^P$) can be easily removed by dust collection. Furthermore oxidized mercury is soluble in water and easily adsorbed on solid surfaces to achieving its removal [7]. However $Hg^0$ is neither soluble in water nor easily adsorbed. It has a lifetime of 1–2 years in the atmosphere and can be transported over long distances to cause global mercury pollution. Therefore, removal of $Hg^0$ emitted from the flue gas has been a great challenge to minimizing the emission of mercury.

Various processes, such as oxidant injection, catalytic oxidation, and photocatalytic oxidation, were developed for the removal of $Hg^0$ in the flue gas [8–14]. Recently, the progress in the photocatalytic oxidation of $Hg^0$ gave us a new sight for this novel method [15,16]. Due to the great efforts of Wu et al., $TiO_2$-based nano-particles such as $TiO_2$ doped on silica gel, $SiO_2$–$TiO_2$ nano-composites and $SiO_2/V_2O_5/TiO_2$ composite catalyst, have demonstrated greater than 90% $Hg^0$ removal under UV irradiation in room conditions [17–20]. With the following studies by Lee and co-workers [21–23], the effects of flue gas components on the photocatalytic oxidation of Hg capture were also studied. They also found that the removal of $Hg^0$ based on a photocatalytic oxidation–adsorption mechanism. The oxidized Hg on the photocatalyst surface would be a great benefit to the proceeding adsorption of $Hg^0$.

For the development of second-generation photocatalyst, the structure modification of catalyst currently remains to be an important issue [24–29]. $TiO_2$ nanotubes (TNTs), which have unique tubular structures and large surface area might be a wonderful photocatalyst for the removal of $Hg^0$. In this paper, TNTs was synthesized by a hydrothermal method under the different calcination temperatures. The photocatalytic performance and $Hg^0$ adsorption ability investigation of TNTs were based on the $Hg^0$ removal experiments in simulated flue gas. With the analysis of physicochemical properties, the relationship between the activity, calcination temperature, and tubular structure was discussed.

* Corresponding author at: Department of Environmental Engineering, Zhejiang University, Hangzhou 310058, China. Tel.: +86 571 88982863; fax: +86 571 87953088.
*E-mail address:* zbwu@zju.edu.cn (Z. Wu).

0920-5861/$ – see front matter © 2011 Published by Elsevier B.V.
doi:10.1016/j.cattod.2011.03.006

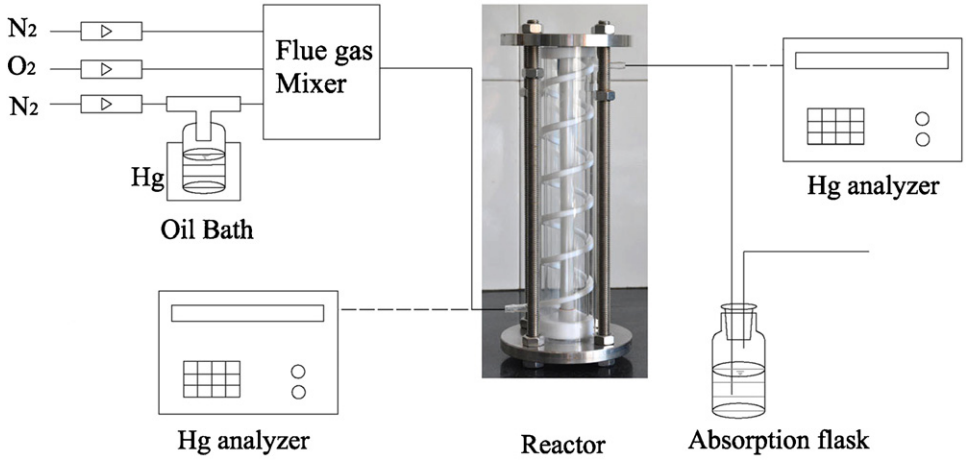


**Fig. 1.** The schematic diagram of the experimental system.

## 2. Experimental

### 2.1. Preparation of TNTs

The titania nanotubes (TNTs) were synthesized by a hydrothermal method which was developed by Kasuga et al. [28] In typical preparation process, 2.0 g $TiO_2$ powder (P25, Degussa AG, Germany) was mixed with 70 mL of 10 M NaOH aqueous solution by magnetic force. The solution was moved into a 100 mL polyflon (PTFE) autoclave at 150 °C for 24 h as follow. After that, the slurry was filtrated and washed with 0.1 M HCl solution and distilled water until the pH value of the rinsing solution reached 6.5. Finally, the washed samples were dried at 80 °C for 12 h, and further calcined at four different temperatures (300 °C, 400 °C, 500 °C and 600 °C) for 1 h in air to get four types of TNTs (presented as TNTs – *x*, *x* was the calcination temperature).

### 2.2. Characterization of catalysts

X-ray diffraction analysis (XRD) of the catalysts was performed on a Rigaku diffractometer (D/Max RA) at 40 kV and 150 mA (Cu Kα = 1.542 Å), at an angle of 2$\theta$ from 10° to 80°. The scan speed was 1°/min. The morphology, structure and crystal size of the samples were examined by scanning electron microscope analysis (Sirion200, USA) and transmission electron microscopy (JEM-2010, Japan). Analysis of the surface element distributions of the fresh samples and the adsorbed mercury compound on the used samples was conducted by X-ray photoelectron spectroscopy (Thermo ESCALAB 250, USA). The specific surface area of the samples was determined by Brunauer-Emmett-Teller (BET) method (ASAP 2020, USA).

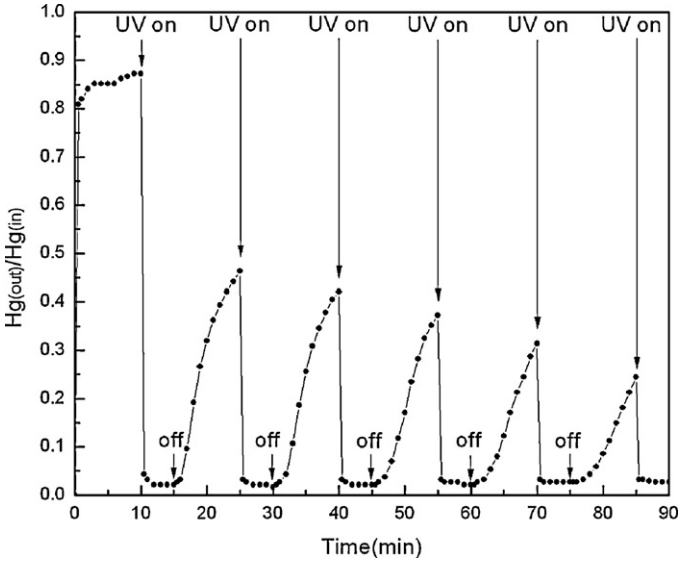


**Fig. 2.** Fractional $Hg^0$ outlet concentration for Degussa P25.

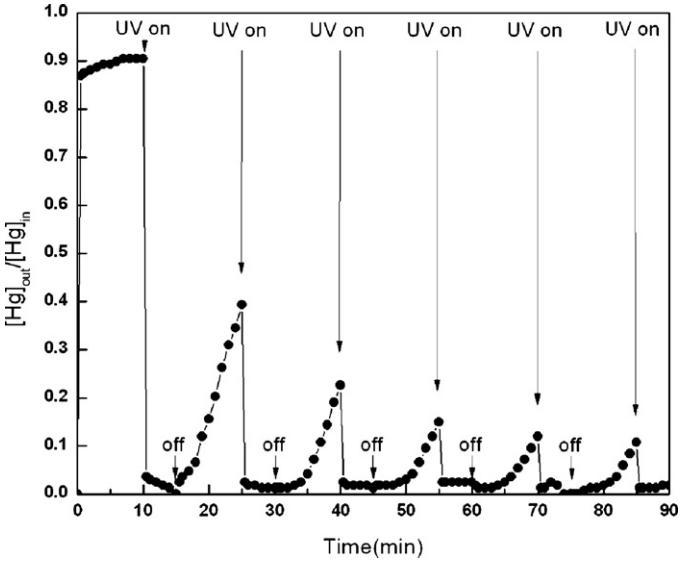


**Fig. 3.** Fractional $Hg^0$ outlet concentration for TNTs-400.

### 2.3. Experimental studies

Fig. 1 shows a schematic diagram of the experimental system. The simulated flue gas was consisted of three gas flows, pure

**Table 1**
Physical properties of the prepared TNTs.

| Calcination temperature (°C) | $S_{BET}$ ($m^2$/g) | Pore volume ($cm^3$/g) | Pore size (Å) |
|---|---|---|---|
| Uncalcined | 337 | 1.28 | 145 |
| 300 °C | 357 | 1.36 | 152 |
| 400 °C | 146 | 1.20 | 329 |
| 500 °C | 119 | 1.06 | 358 |
| 600 °C | 74 | 0.84 | 455 |

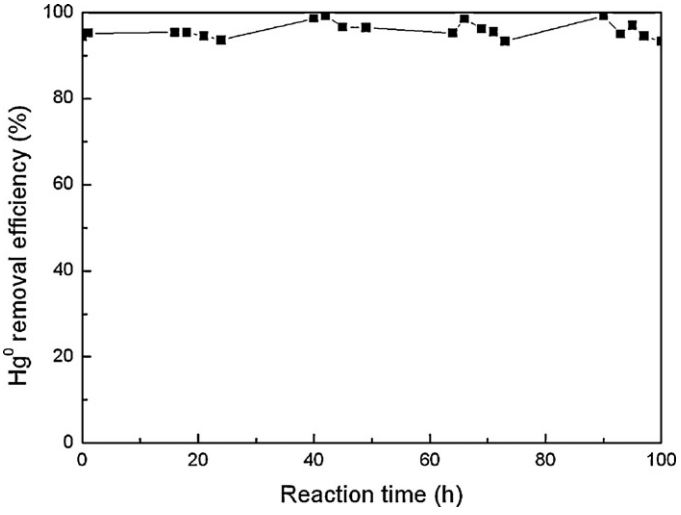


**Fig. 4.** 100 h photocatalytic reaction for TNTs-400.

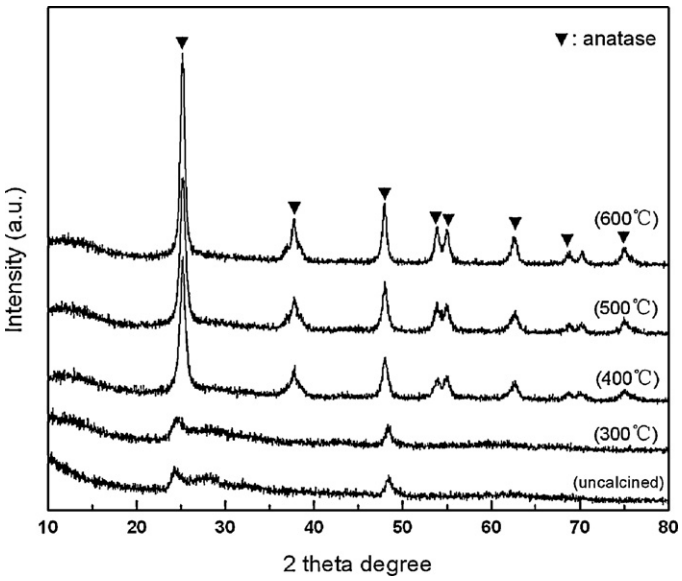


**Fig. 6.** XRD patterns of TNTs calcined at different temperatures.

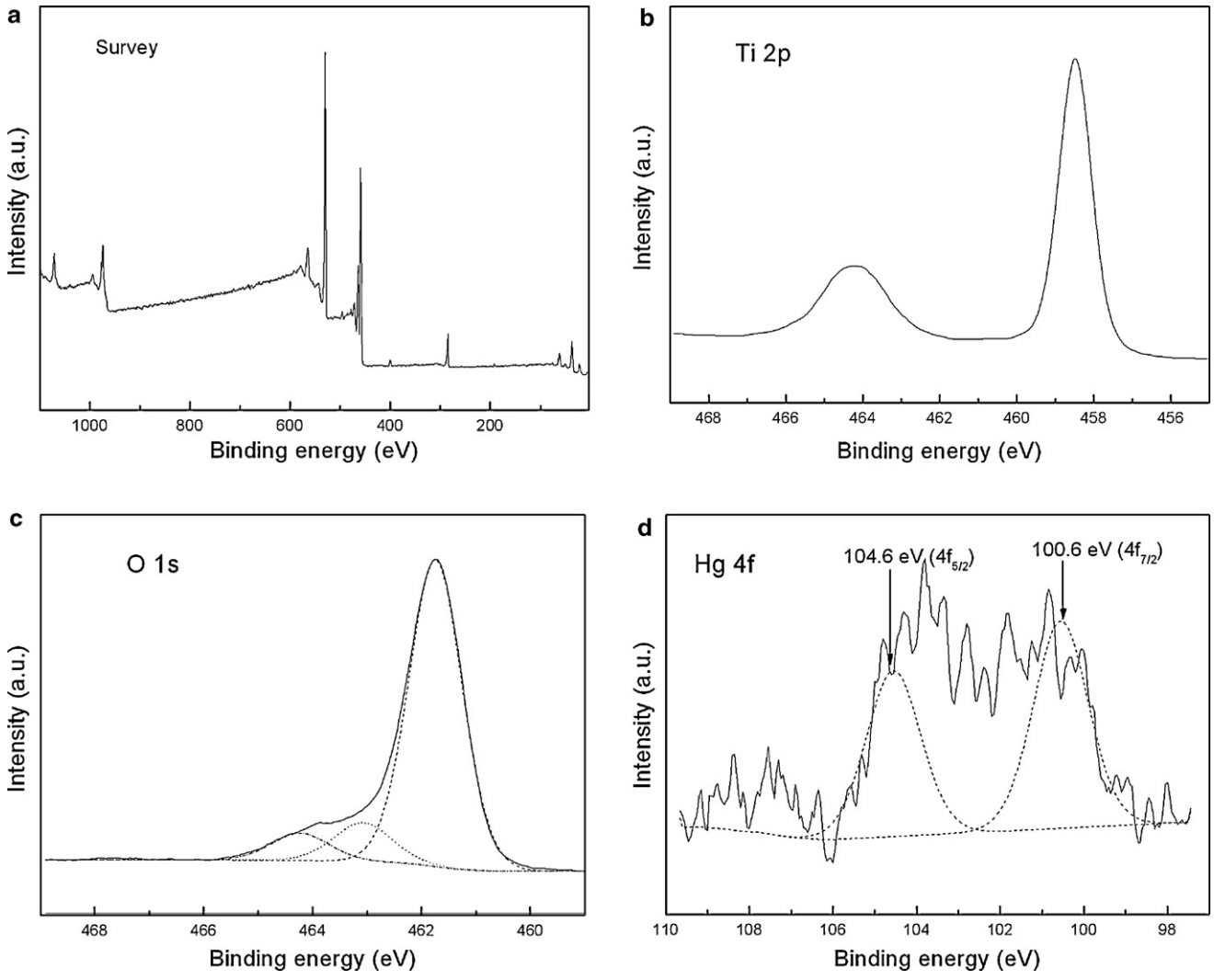


**Fig. 5.** XPS spectra of the used TNTs (a. survey spectra, b. Ti2p band, c. O1s band, d. Hg4f band).

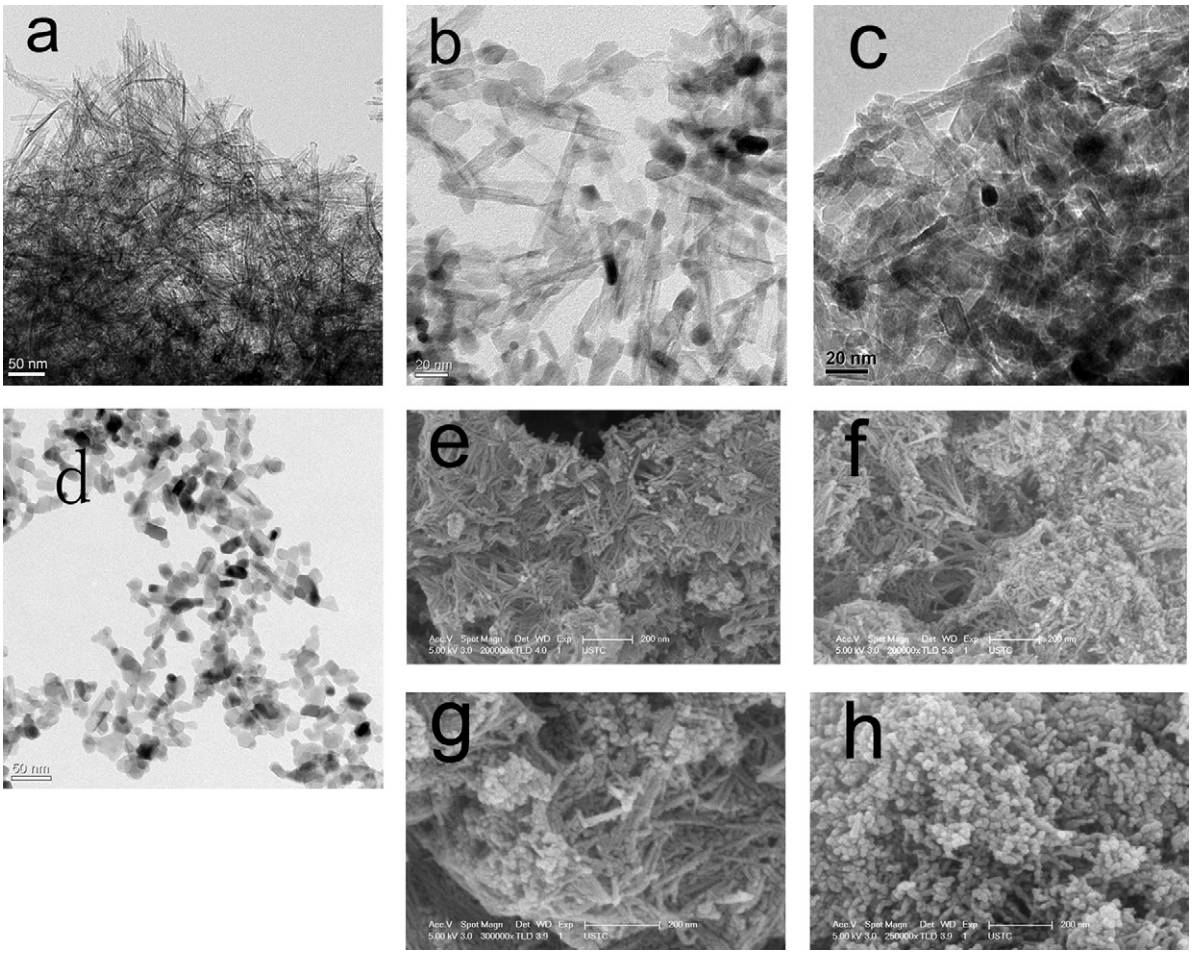


**Fig. 7.** TEM images of TNTs: (a) uncalcined, (b) TNTs-400, (c) TNTs-500, (d) TNTs-600; and SEM images of TNTs: (e) uncalcined, (f) TNTs-400, (g) TNTs-500, (f) TNTs-600.

$N_2$ was divided into two streams as the carrier gas and dilution gas, and third gas stream was $O_2$. The carrier gas stream passed through the surface of a liquid $Hg^0$ reservoir and introduced $Hg^0$-vapor-laden air into the system. The $Hg^0$ reservoir was placed in an oil bath (70 °C) to maintain a constant $Hg^0$ vapor pressure. The reactor was a ringlike fixed-bed photocatalytic reactor, which included two concentric quartz glass tubes (Ø 6.2 cm × 32 cm, Ø 5.0 cm × 32 cm) and a spiral polyflon stand rotated with the inner quartz glass tube in order to dispersing the gas flows. UV lamp (20 W, λ = 365 nm) set on the centerline of reactor. The catalysts were doped on a strip of woven glass fabric used a dip-coating method that reported in our previous work [30]. The coated fabric was rotated around the inside quartz glass tube and fixed on the polyflon stand as well. In all experiments, the weight of catalyst coated was kept to be 0.6 g ± 10%. In a typical condition, the simulated flue gas ($O_2$ concentration: 5%) passed through the reactor at a flow rate of 1.0 L/min with an empty bed retention time (EBRT) of 12.6 s.

Cold vapor atomic absorption spectrophotometry analyzer (SG921, Jiangfen, China) was used as the continuous monitor to measure the inlet and outlet $Hg^0$ concentration continuously, and the data was recorded with a data acquisition system (N-2000, China). A dilution gas (v/v = 1:1) was also introduced into Mercury analyzer (Lumex, Russia) to certifing the $Hg^0$ concentration in the simulated flue gas. The inlet $Hg^0$ concentration in this work was between 300 ± 15 μg/m$^3$.

## 3. Results and discussion

### 3.1. Photocatalytic oxidation–adsoprtion behavior of TNTs-400

The photocatalytic oxidation–adsorption experiment was similar to the experiment of Wu et al. [17–20]. The inlet and outlet $Hg^0$ concentration were measured continuously. At first, the simulated flue gas was passed through the reactor for 10 min and the initial adsorption capacity of $Hg^0$ was recorded. Then, UV light was turned on for 5 min-photocatalytic oxidation stage of $Hg^0$, and then turned off for 10 min-adsorption stage for $Hg^0$. Another five UV on/off cycles were repeated, and the final $Hg^0$ removal efficiency was recorded. Fig. 2 is the oxidation–adsorption behavior for P25. After five cycles, the adsorption capability of P25 was significantly improved, but the adsorption efficiency of final section was only reached 80 percentages. Due to the economic performance of our technology, it is important to improve the adsorption capability of catalyst.

As shown in Fig. 3, the TNTs, which calcined at 400 °C were used for six cycles of adsorption/photocatalytic oxidation. The catalyst showed a small initial adsorption capacity for $Hg^0$ in the first 10 min adsorption stage without the irradiation of UV light. In the followed photocatalytic oxidation phase stage, the outlet $Hg^0$ concentration quickly dropped when the UV light was turned on and maintained at a low level during this 5 min. The outlet $Hg^0$ concentration decreased to 50% of first adsorption stage in the end of

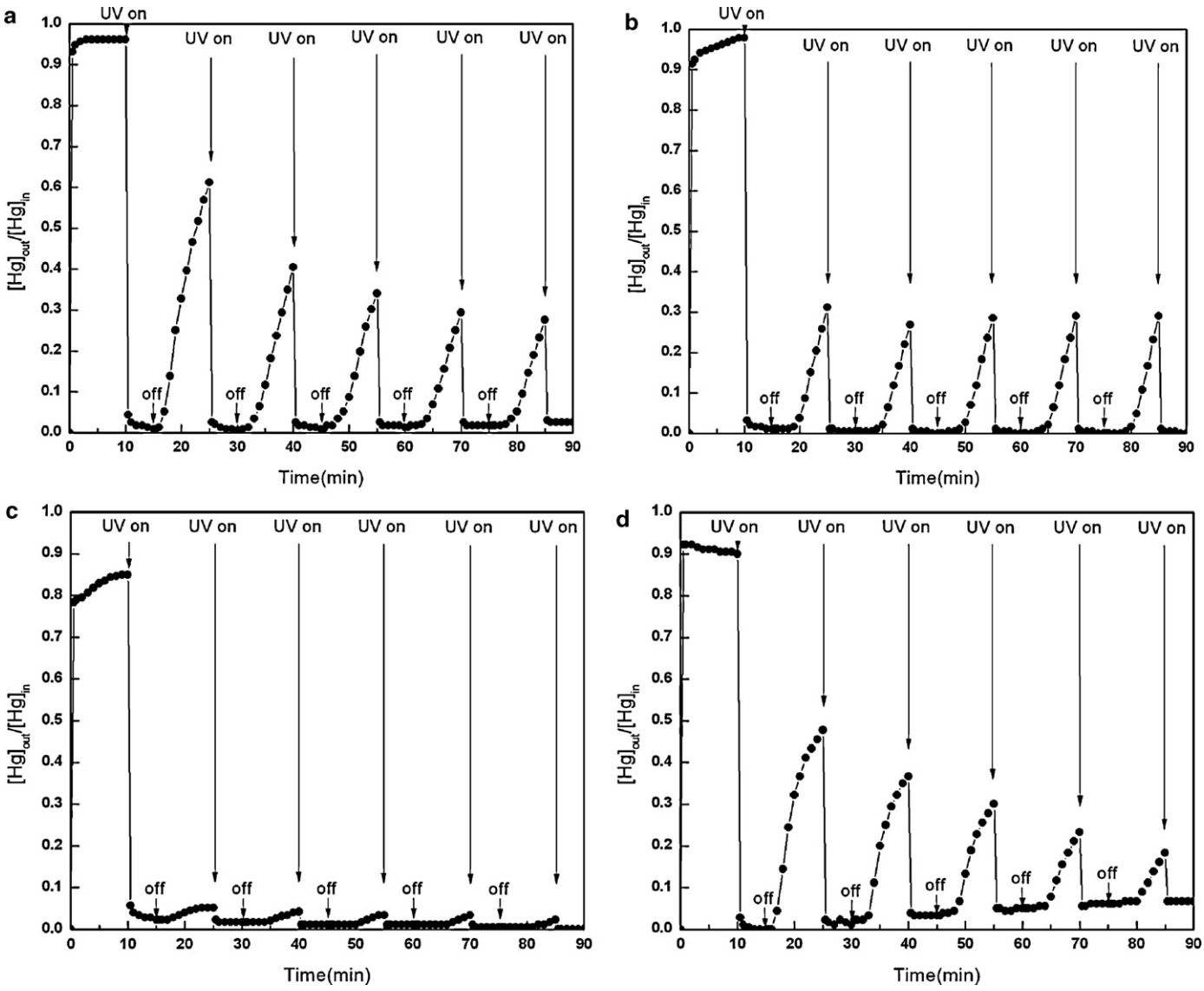


**Fig. 8.** Fractional $Hg^0$ outlet concentration for TNTs calcined at different temperatures (a. uncalcined, b. TNTs-300, c. TNTs-500, d. TNTs-600).

second adsorption phase. In the photocatalytic oxidation stages, the removal efficiencies were always high (near 100%). But an obvious increasing trend was investigated in the ordinal adsorption stage. The $Hg^0$ removal efficiency was more than 90% even without UV irradiation in the final cycle. It was suggested that the synergy effect existed between photocatalytic oxidation and adsorption, similar to the theory proposed by Wu et al. [17,18,21]. With the tubular morphology of the TNTs, vast surface area and diverse pore structure were provided. Abundant hydroxyl (OH) radicals were generated on TNTs surface with the UV irradiation, which could immediately react with $Hg^0$ to form HgO. Thus high removal efficiency could be easily achieved when the UV light was on. Some of the generated HgO deposited on the surface and the pore of catalyst. Because of the high affinity between $Hg^0$ and HgO, the deposited HgO decreased the contact angle between $Hg^0$ and catalyst, and enhanced the adsorption of $Hg^0$. Then the adsorbed $Hg^0$ will be oxidized to HgO in next photocatalytic oxidation phases to capturing more $Hg^0$.

In order to confirm this mechanism, the TNTs-400 was continually reacted for 100 h in accordance with the cyclic model mentioned before (Fig. 4). The $Hg^0$ removal efficiency of TNTs-400 maintained at 90% during 100 h reaction. X-ray photoelectron spectroscopy was performed to study the surface element distributions of the used TNTs. Fig. 5d presents the XPS spectra in the Hg4f region. The peaks located at 100.6 and 104.6 eV ($4f_{7/2}$ and $4f_{5/2}$) were corresponding to oxidized mercury (HgO) [7]. The presence of HgO in the used TNTs indicated that the photocatalytic oxidation of $Hg^0$ was occurred and the generated HgO was partly deposited on TNTs.

### 3.2. Crystal structure and morphology of TNTs

Fig. 6 shows the XRD patterns of the TNTs calcined at different temperatures. The uncalcined TNTs and TNTs-300 showed two vague peaks located at the $2\theta$ degree of 25.2° and 62.58°, which were announced to anatase phase. Obviously, anatase crystals were few in original nanotubes, and anatase crystal could not formed by calcination at 300 °C. With the increase of calcination temperature, the anatase crystals were formed and enlarged, according to the obvious appearance of anatase phase peaks, which were observed at the $2\theta$ degree of 25.2°, 37.8°, 47.98°, 54.0°, 55.06°, 62.58°, 68.9° and 75.18°. The anatase phase of TNTs was the preferred crystalline for the photocatalytic reaction, which provided the excellent photocatalytic capability.

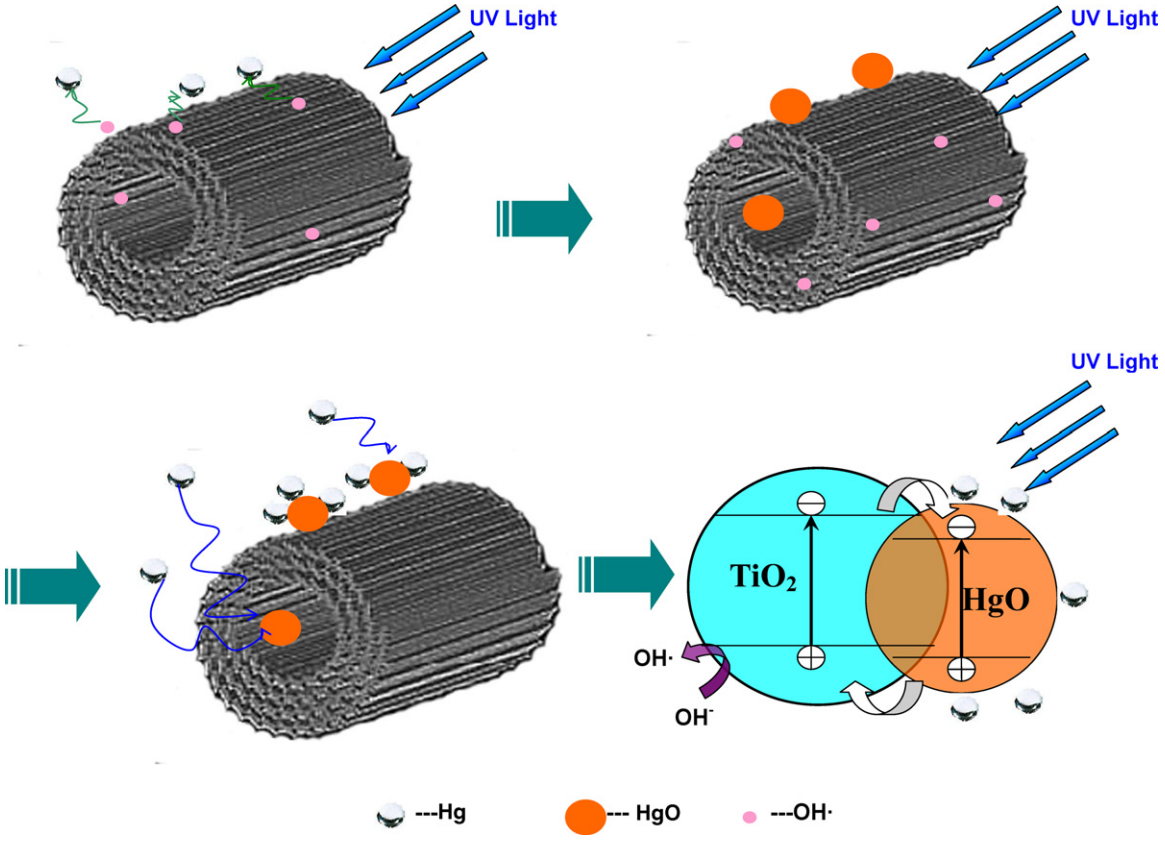


**Fig. 9.** Photocatalytic oxidation and absorption mechanism for TNTs.

Due to the hybrid photocatalytic oxidation–adsorption reaction, the removal efficiency was controlled not only by crystal phase of the catalysts but also the morphology of catalysts. Table 1 list the surface area and pore size of these prepared TNTs. The surface area and pore volume were decreased with the calcination temperature; and on the contrary the pore diameter was increased.

TEM and SEM images (Fig. 7) are shown for uncalcined TNTs, TNTs-400, TNTs-500 and TNTs-600. The nanotube structure was clearly observed in uncalcined TNTs. In the 400 °C-treared and 500 °C-treared nanotubes, some rodlike particles were observed beside nanotubes. Increasing the temperature to 600 °C, the nanotubes were completely transformed to rodlike particles, which indicated the sintering of tubes.

### 3.3. Removal capacity of TNTs with different calcination temperature

The structure and crystal phase of TNTs would vary with calcination temperature [11]. The TNTs were calcined at 300 °C, 400 °C, 500 °C and 600 °C respectively to finding out the optimum synthesis conditions. In Fig. 8, the TNTs prepared by different calcination temperatures (uncalcined, 300 °C, 500 °C and 600 °C) were used as photocatalyst and adsorbent for six cycle reaction of adsorption/photocatalytic oxidation. These tested samples had the excellent $Hg^0$ removal efficiencies, even the uncalcined nanotubes obtained good removal efficiency above 70% in the last cycle. Thus it was verified that the nanotube structure could enhance the synergistic effect between the photocatalytic oxidation and the adsorption. Combined with Fig. 3, the best removal efficiency was obtained at 500 °C, and then the efficiency tends to be decreased with further high calcination temperature. With the increasing of calcination temperature, the surface area and pore volume decreased. Therefore the deposition sites of HgO might relatively less in the TNTs with high calcination temperature compare to the TNTs with low calcination temperature. But as shown in Figs. 3 and 8, the $Hg^0$ adsorption capacity of TNTs calcined at high temperature (except 600 °C) was larger than that of TNTs calcined at low temperature. The increase of pore diameter might provide an opened pore structure to enlarge the adsorption capacity of TNTs calcined at high temperature. Furthermore, the nanotubes were completely sintered to rodlike particles with 600 °C calcination, thus the advantage provided by nanotubes structure was disappeared.

We proposed the mechanism of photocatalytic oxidation and absorption reaction on TNTs and showed it in Fig. 9. In the photocatalytic oxidation section, abundant hydroxyl (OH) radicals were generated on TNTs surface with the UV irradiation. It could immediately react with $Hg^0$ to form HgO. Also the generated HgO were deposited on the surface and the pore of catalyst. In the adsorption section, the deposited HgO decreased the contact angle between $Hg^0$ and catalyst because of the high affinity between $Hg^0$ and HgO. Thus the adsorption capability of $Hg^0$ was enhanced. Furthermore, mercury oxide deposited on TNTs surface is also a semiconductor, which can form composite semiconductor to improving the photocatalytic activity. In next photocatalytic oxidation stage, the adsorbed $Hg^0$ will be oxidized to HgO for capturing $Hg^0$. These above were responsible for the increasing tendency of mercury removal efficiency. As reported in the literature, the vapor of HCl could release the HgO deposit on the catalyst surface successfully [11]. Furthermore, the solution of HCl also could wash down the HgO on the surface of used TNTs catalyst. Thus, the vapor of HCl and the solution of HCl could be use as the potential regeneration methods for the used TNTs with HgO.

## 4. Conclusion

In this study, titania nanotubes with vast surface area and high porosity were used for the removal of $Hg^0$ in the flue gas. It was verified that the nanotube structure could enhance the synergistic effect between the photocatalytic oxidation and the adsorption. The TNTs samples showed an excellent removal efficiency (>90%) for 100 h, and this high removal efficiency was ascribed to the synergistic effect between the photocatalytic oxidation and adsorption. With the calcination temperature of 500 °C, the TNTs showed the best removal performance of elemental mercury. The nanotubes structure was sintered to rodlike particles with 600 °C calcination, and then the removal efficiency of TNTs-600 was decreased.

## Acknowledgment

This research was financially supported by the National Natural Science Foundation of China (NSFC-50808156), the National High-Tech Research and Development Program (863) of China (2007AA06Z340-3, 2007AA06Z340-4), the Changjiang Scholar Incentive Program (Ministry of Education, China, 2009), the Chinese Post-Doctoral Research Fund Special Funded Projects (200902637) and the Zhejiang Education Agency Project (Y200805367).

## References

[1] T.D. Brown, D.N. Smith, R.A. Hargis Jr., W.J. O'Dowd, J. Air Waste Manage. Assoc. 49 (1999) 628–640.
[2] D.G. Streets, J. Hao, Y. Wu, J. Jiang, M. Chan, H. Tian, X. Feng, Atmos. Environ. 39 (2005) 7789–7806.
[3] S. Wang, L. Zhang, G. Li, Y. Wu, J. Hao, N. Pirrone, F. Sprovieri, M. Ancora, Atmos. Chem. Phys. 10 (2010) 1183–1192.
[4] S. Qiao, J. Chen, J. Li, Z. Qu, P. Liu, N. Yan, J. Jia, Ind. Eng. Chem. Res. 48 (2009) 3317–3322.
[5] S. Li, C. Cheng, B. Chen, Y. Cao, J. Vervynckt, A. Adebambo, W. Pan, Energy Fuels 21 (2007) 3292–3299.
[6] Y. Cao, Z. Gao, J. Zhu, Q. Wang, Y. Huang, C. Chiu, B. Parker, P. Chu, W. Pan, Environ. Sci. Technol. 42 (2008) 256–261.
[7] W. Lee, G. Bae, Environ. Sci. Technol. 43 (2009) 1522–1527.
[8] A.A. Presto, E.J. Granite, Environ. Sci. Technol. 40 (2006) 5601–5609.
[9] Y. Cao, B. Chen, J. Wu, H. Cui, J. Smith, C. Chen, P. Chu, W. Pan, Energy Fuels 21 (2007) 145–156.
[10] Y. Cao, Y. Duan, S. Kellie, L. Li, W. Xu, J.T. Riley, W. Pan, Energy Fuels 19 (2005) 842–854.
[11] J. Li, N. Yan, Z. Qu, S. Qiao, S. Yang, Y. Guo, P. Liu, J. Jia, Environ. Sci. Technol. 44 (2010) 426–431.
[12] Z. Qu, N. Yan, P. Liu, Y. Chi, J. Jia, Environ. Sci. Technol. 43 (2009) 8610–8615.
[13] Z. Qu, N. Yan, P. Liu, Y. Guo, J. Jia, Environ. Sci. Technol. 44 (2010) 3889–3894.
[14] Z. Qu, J.J. Chang, T. Hsiung, N. Yan, H.P. Wang, R. Dod, S. Chang, C. Miller, Energy Fuels 24 (2010) 3534–3539.
[15] E.J. Granite, H.W. Pennline, J.S. Hoffman, Ind. Eng. Chem. Res. 38 (1999) 5034–5037.
[16] C.R. McLarnon, E.J. Granite, H.W. Pennline, Fuel Process. Technol. 87 (2005) 85–89.
[17] C. Wu, T. Lee, G. Tyree, E. Arar, P. Biswas, Environ. Eng. Sci. 15 (1998) 137–148.
[18] E. Pitoniak, C. Wu, D. Londeree, D. Mazyck, J. Bonzongo, K. Powers, W. Sigmund, J. Nanopart. Res. 5 (2003) 281–292.
[19] Y. Li, C. Wu, Environ. Sci. Technol. 40 (2006) 6444–6448.
[20] Y. Li, P. Murphy, C. Wu, K. Powers, J. Bonzongo, Environ. Sci. Technol. 42 (2008) 5304–5309.
[21] S. Rodriguez, C. Almquist, T. Lee, M. Furuuchi, E. Hedrick, P. Biswas, J. Air Waste Manage. Assoc. 54 (2004) 149–156.
[22] T. Lee, P. Biswas, E. Hedrick, Ind. Eng. Chem. Res. 43 (2004) 1411–1417.
[23] S. Jeon, Y. Eom, T. Lee, Chemosphere 71 (2008) 969–974.
[24] X. Sun, Y. Li, Chem. Eur. J. 9 (2003) 2229–2238.
[25] Z. Wu, F. Dong, W. Zhao, H. Wang, Y. Liu, B. Guan, Nanotechnology 20 (2009) 235701.
[26] F. Dong, W. Zhao, Z. Wu, Nanotechnology 19 (2008) 365607.
[27] Y. Hou, X. Li, X. Zou, X. Quan, G. Chen, Environ. Sci. Technol. 43 (2009) 858–863.
[28] T. Kasuga, M. Hiramatsu, A. Hoson, T. Sekino, K. Niihara, Langmuir 14 (1998) 3160–3163.
[29] C. Ratanatawanate, C. Xiong, K.J. Balkus Jr., ACS Nano 2 (2008) 1682–1688.
[30] H.Q. Wang, Z.B. Wu, W.R. Zhao, B.H. Guan, Chemosphere 66 (2007) 185–190.